Low Density Water Structure Observed in a Nano-Segregated Cryoprotectant Solution at Low Temperatures from 285 K to 238 K

J.J. Towey[†], A.K. Soper[‡], and L. Dougan[φ]

† Faculty of Engineering, University of Nottingham, Nottingham, NG7 2NR, UK
‡ ISIS Facility, Rutherford Appleton Laboratory, Chilton, Didcot, Oxon, OX11 OQX, UK
φ School of Physics and Astronomy, University of Leeds, Leeds, LS2 9JT, UK

Email: L.Dougan@leeds.ac.uk
Telephone: +44 113 343 8958

ABSTRACT: Liquid water structure is defined by its molecular association through hydrogen bonding. Two different structures have been proposed for liquid water at low temperatures, low density liquid (LDL) and high density liquid (HDL) water. Here we demonstrate a platform which can be exploited to experimentally probe the structure of liquid water in equilibrium at temperatures down to 238 K. We make use of a cryoprotectant molecule, glycerol which when mixed with water lowers the freezing temperature of the solution non-monotonically with glycerol concentration. We use a combination of neutron diffraction and computational modeling to examine the structure of water in glycerol - water *liquid* mixtures at low temperatures from 285 K to 238 K. We confirm that the mixtures are nano-segregated into regions of glycerol-rich and water-rich clusters. We examine the water structure and reveal that at the temperatures studied here, water forms a low density water structure which is more tetrahedral than that at room temperature. We postulate that nano-segregation allows water to form a low density structure which is protected by an extensive and encapsulating glycerol interface.

INTRODUCTION

Liquid water plays a fundamental role in life on Earth.[1] Covering a wide temperature and pressure range, water's presence is crucial for a vast range of biological,[2] geological[3] and environmental processes.[4] Despite this importance and ubiquity a full understanding of its dynamical and structural properties remains lacking.[5-6] Liquid water exhibits many anomalies in its thermodynamic properties, including a high capacity, high thermal conductivity and density maximum at 277.15 K.[5,7-8] The unusual features of liquid water are more enhanced at lower temperatures and may result from the local tetrahedral ordering due to hydrogen bonding.[8] Among the many theoretical approaches developed to explain water properties the liquid-liquid critical point (LLCP) hypothesis[9] has been explored by a number of experimental[10-18] and computational studies.[19-20] Although heavily criticized[21], the LLCP hypothesis builds on the idea that at some low temperature and pressure, unavailable to the stable bulk liquid phase, water, driven by hydrogen bond interactions between water molecules, separates into two phases, a low density phase with an open tetrahedrally coordinated hydrogen bond network, and a high density, phase where the hydrogen bonds are more distorted. The extension of the properties of this hypothetical second critical point in water is then used to explain the anomalous properties of the stable liquid phase.

The LLCP hypothesis advocates the continuation of the local structure of water into its amorphous solid phases, low density amorphous (LDA) and high density amorphous (HDA) ice.[22] LDA and HDA can be accessed by reducing the temperature below the glass transition temperature of water $T_g \sim 130$ K and applying a pressure of order 1GPa.[8] They can be transformed from one amorphous phase to the other by tuning the pressure[23], so displaying polymorphism.[22] Under this same scenario the liquid state below the hypothetical LLCP is regarded as a mixture of two liquid structures, one referred to as low density liquid (LDL) water and the other high density liquid (HDL) water.[9] In the LLCP hypothesis, water anomalies are a result of the competition between the two liquid forms, LDL and HDL water. However to date, there has been no confirmed verification of the LLCP hypothesis in either the bulk liquid or when heavily confined in a porous matrix.

To validate this hypothesis, experiments are needed which can observe water at low temperatures. Accessing liquid water at low temperatures is challenging however, due to

the ready formation of the stable phase Ice Ih.[24] One approach is to use nano-confined water.[24-27] By confining water in nanoporous structures, neutron and Raman scattering and NMR spectroscopy have examined water at low temperatures. For example, confining water in a nanoporous structure, the vibrational spectra of deeply supercooled water was measured by Fourier transform infrared spectroscopy in the temperature range 183 < T < 273 K. This study claimed to provide evidence of the existence of LDL water in supercooled, confined water.[16] Neutron scattering experiments attempted to measure the density of heavy water confined in a nanoporous silica matrix in a temperature range from 130 < T < 300 K and a pressure range from 1 < P < 2900 bar.[28] The study measured a density hysteresis which was interpreted to support the LLCP hypothesis. However, these findings have been open to criticisms that the behavior of the water may be altered by the silica pore surfaces or that water is confined in narrow nanopores, rather than being in the bulk state.[27] Previous experimental studies have provided access to low density water by exploring the relevant region of the stable P-T phase diagram, then extrapolating these data into the metastable region. For example, neutron diffraction experiments at 268 K as a function of pressure were extrapolated into the metastable liquid and indicated an open, hydrogen bonded tetrahedral structure for low density metastable water [18]. In another study small angle x-ray scattering is claimed to demonstrate the presence of density fluctuations in water at temperatures from 280.15 K to 347.15 K.[12] The authors proposed that the density difference contrast is due to fluctuations between tetrahedral-like and hydrogen bond distorted structures, related to LDL and HDL water. However, the detailed structure of the two types of species reported in that study was not determined, and a countering study, claimed there was no evidence for these structures.[29] Yet another study has followed the structural evolution of supercooled water in 10μm sized droplets to 227 K and found a near-linear trend of increasing tetrahedrality as the temperature was lowered. [30-31] High pressure studies have probed the dynamics associated with low-density and high-density forms of liquid water, using FTIR to monitor the line shape of the OD stretching mode of HOD as a function of pressure.[32] While Raman spectroscopy experiments on glycerol-water solutions have observed pressure-incuded 'polymorphic transition in the glycerol-water solution, which is thought to relate to water polyamorphism. [33] However, to date, attempts to obtain structural information on supercooled water under pressure using techniques such as neutron diffraction have been challenging. Studies by Bellissent-Funel made use of emulsions of D$_2$O/deuteroheptane/sorbitan to allow neutron diffraction experiments to be completed at pressures of 2600 bar and at temperatures down to 208 K. [34] An experimental approach is needed which provides access to the *stable* liquid structure at low temperatures, and in particular, one which is sensitive to hydrogen bonding. Information on the structure of the hydrogen bonded liquid is essential in describing LDL and HDL water, if they exist. In the present study we describe such an approach.

We exploit the use of cryoprotectant solutes which depress the freezing point and inhibit ice formation. Cryoprotectants are substances that are used to protect biological molecules, tissues and organs from the freezing damage that occurs due to ice formation at low temperatures.[35] Some cryoprotectants are utilized for their ability to lower the glass transition temperature of a solution or system, preventing the freezing that would occur in their absence.[35-36] Since many cryoprotectants can hydrogen bond with biological molecules in solution, they can effectively take the place of water molecules in providing lubrication, maintaining the necessary flexibility needed for function and stability. Here we use the conventional cryoprotectant glycerol. While pure glycerol freezes at a temperature of 290.95 K at ambient pressure, when mixed with water it exhibits a minimum in the freezing point depression[37] of 226.65 K at mole fraction glycerol x_g = 0.28 (Figure 1). Glycerol has been used as a cryoprotectant for many decades to reduce ice formation in sperm, oocytes and embryos that are stored in liquid nitrogen.[38-39] This cryoprotectant is also used in nature, where for example Artic salamanders produce glycerol in their livers for use as a cryoprotectant [40]. Glycerol use is not just limited to cryopreservation. This molecule has been utilized in a wide range of applications in the pharmaceutical and food industry[41-43] and more recently as a solvent for green chemistry.[44] While glycerol was the first cryoprotectant molecule to be discovered[45], the molecular mechanisms by which it acts to prevent freezing damage still remain unclear. Central to this problem is the action of glycerol on the structure of water at low temperatures. Hence determining the structural properties of water in cryoprotectant solutions at low temperatures is an important step in understanding this process.

While there have been a large number of computational studies on glycerol and glycerol-water mixtures, including [36, 46-64], experimental studies yielding information on liquid structure are more limited.[56, 65-66] In the last 4 years we have completed experimental, structural studies of pure glycerol and glycerol-water mixtures at 298 K using a combination of neutron diffraction and computational modeling.[67-71] Our studies have shown that at intermediate concentrations (between x_g = 0.25 to 0.50) the mixture segregates on the nanometer length scale to form water-rich and glycerol-rich clusters.[70-71] This nano-segregation results in regions which exist as hydrogen bonded clusters which differ in size across the concentration range. In the concentrated glycerol region (x_g = 0.80) a large glycerol cluster exists which spans the full size of the system. Conversely, the majority of the water (56 %) occurs as isolated water molecules. This preference for isolated water molecules results in a well-mixed solution with a considerable glycerol-water interface. In the dilute glycerol region (x_g = 0.05) there is instead a prevalence of isolated glycerol molecules (40 %), again resulting in a mixture with a large glycerol-water interface. An interesting regime was found to exist, however, at the intermediate glycerol concentrations (between x_g = 0.25 to 0.50).

Between a concentration of $0.25 \leq x_g \leq 0.50$ a solution exists which is composed of both glycerol clusters and water clusters which span the entire system. These clusters are large in size and are fully percolating. Given the presence of both glycerol- and water percolating clusters, this intermediate regime is referred to as a bi-percolating cluster regime. Bi-percolation has been observed previously in other binary liquid systems, including methanol-water [72]. At all the concentrations studied at room temperature, water was found to maintain its hydrogen bonding ability, forming around 4 hydrogen bonds per molecule[70]. This is achieved by a balance

between forming water-water and water-glycerol hydrogen bonds. Thus the hydrogen bonding of glycerol and water allow both species to exist as percolating networks in the system, while maintaining their hydrogen bonding ability.
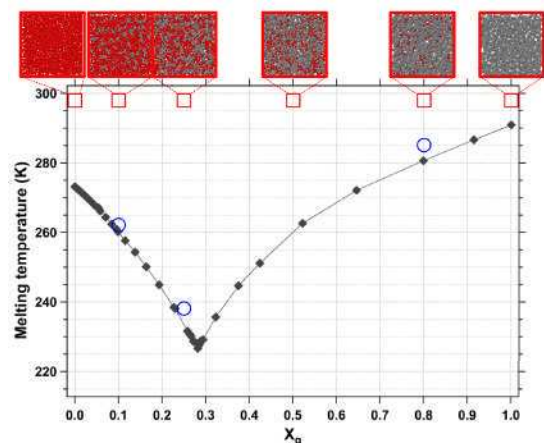

Figure 1: The equilibrium melting temperature of aqueous glycerol as a function of glycerol mole fraction (x_g) is shown by the black symbols and line, taken from the literature.[37] The lowest melting temperature is at a concentration of x_g = 0.28. Red squares show the concentration of glycerol-water mixture studied previously at 298 K[59, 67] and blue circles show the temperature and concentration of each of the low temperature neutron diffraction experiments.

Given the detailed information gained from the concentration-dependent room temperature studies [67, 69-71], three concentrations are of interest for further study. Firstly, the concentrated mixture of x_g = 0.80, in which at room temperature glycerol is forming a percolating network and water molecules must be accommodated at the glycerol-water interface and within small water clusters of 2-7 molecules. Secondly, a dilute mixture of x_g = 0.10 in which water is forming a percolating network. Thirdly, an intermediate concentration of x_g = 0.25 in which both glycerol and water are percolating. For each of these concentrations, we completed neutron diffraction experiments at low temperatures for glycerol-water solutions; glycerol mole fraction, x_g = 0.10 at 262 K , x_g = 0.25 at 238 K and x_g = 0.80 at 285 K, (Figure 1). We determined (i) if nano-segregation persists at low temperatures and (ii) the structure of any water clusters at temperatures of 285 K, 262 K and 238 K.

METHODS

Neutron diffraction experiments.

The neutron diffraction experiments were completed on the small angle neutron diffractometer for amorphous and liquid samples (SANDALS) time-of-flight diffractometer at the ISIS pulsed neutron facility within the Rutherford Appleton Laboratory, UK. This instrument is optimized for the study of liquid samples containing hydrogen.[73-81] The experimental setup for the liquid sample measurements was similar to that employed in recent measurements of glycerol-water mixtures at room temperature.[70] The standard corrections and normalizations have been applied to the neutron data by means of the program Gudrun.[82] Deuterated samples of water along with protiated and deuteriated samples of anhydrous glycerol were obtained from Sigma-Aldrich and used without additional purification. We completed a detailed structural determination of glycerol-glycerol, glycerol-water and water-water interactions. This has been completed for glycerol-water solutions; glycerol mole fraction, x_g = 0.10 at 262 K, x_g = 0.25 at 238 K and x_g = 0.80 at 285 K, (Figure 1). For each concentration a total of 5 samples were used, making use of relevant isotope substitution of the hydrogen. The 5 isotopic substitutions were (i) Glycerol-D8-D2O (ii) Glycerol-D5-H2O, (iii) Glycerol-D5HD3-HDO, (iv) Glycerol-H8-H2O and (v) Glycerol-HD8-HDO.

Empirical Potential Structural Refinement Analysis

In this study, the technique of Empirical Potential Structural Refinement (EPSR) has been used to build a three-dimensional model of the structure of the liquid that is consistent with the five measured total structure factors.[83] We refer to two distinct atomic components in water and six distinct atomic components in glycerol molecules. In the water molecule, the oxygen atom is labeled O_W, while the hydrogen atom is labeled H_W. In glycerol, the carbon atoms are labeled CC and CG and refer to the central and distal carbon atoms, respectively. The oxygen atom attached to the central carbon atom is labeled OC, while the oxygen atoms bonded to each of the distal carbons are labeled O. The hydrogen atoms are labeled H and HG for the hydroxyl and methyl hydrogen atoms, respectively. A full structural characterization of the system requires the determination of 36 radial distribution functions (RDFs), which is well beyond the capability of any existing diffraction techniques by themselves. To build a model of glycerol and water liquid structure, the experimental data are used to constrain a computer simulation. In an EPSR simulation there are two potentials, the reference potential (RP) based on known or assumed parameters for the intra-molecular and inter-molecular potentials, and the empirical potential (EP), which is obtained directly from the diffraction data.[83] This potential drives the structure of the three-dimensional model toward molecular configurations that are consistent with the measured partial structure factors from the neutron diffraction experiments. EPSR therefore aims to produce a physically realistic model with simulated partial structure factors that fit the experimental results as closely as possible. This method has been applied previously to study pure glycerol and glycerol-water mixtures at room temperature.[67-71] In the present study we examine the structure at low temperature for the first time and compare with the room temperature data. The SPC model was employed as the RP for water molecules.[84] Full details of the other Lennard-Jones and charge parameters for water and glycerol molecules that were used to define the RP are given in the Supporting Information of the room temperature study[70]. Simulation boxes were built with the same molecular ratios as the experiment[70] and used density values from the literature (Tables 1 and 2 in Supporting Information).

RESULTS AND DISCUSSION

Neutron diffraction data on glycerol-water mixtures

Neutron diffraction experiments were completed on the SANDALS instrument at the ISIS Facility using 5 different isotopic substitutions for each of the 3 glycerol-water mixtures at low temperature. Figure 2 shows the neutron diffraction data in the form of a structure factor F(Q) (black circles) for the glycerol-water mixture x_g = 0.10 at 262 K (Figure 2a), x_g = 0.25 at 238 K (Figure 2b) and x_g = 0.80 at 285 K (Figure 2c). The fitted data obtained by the EPSR model for the 3 glycerol-water mixtures is shown in Figure 2 a-c, red line). The agreement of the simulated structure factors is excellent for all 3 mixtures. From the EPSR molecular ensembles, we derive site-site radial distribution functions (RDFs) $g_{\alpha\beta}(r)$, which describe the relative density of one type of atom, type, β, as a function of distance, r, from another atom type, α.

Nano-segregation in glycerol-water mixtures at low temperature

Our previous studies on glycerol-water mixtures at room temperature showed nano-segregation of the system into glycerol-rich and water-rich clusters[67, 69-71]. Here, we determined if nano-segregation persisted at low temperatures. The EPSR generated ensembles were interrogated to extract structural information on glycerol and water clusters in the solution. Representative snapshots from the EPSR simulation of the glycerol–water solution are shown in Figure 3a for glycerol-water mixtures x_g = 0.10 at 262 K, x_g = 0.25 at 238 K and x_g = 0.80 at 285 K. Water molecules are represented by their oxygen atoms (red spheres) and glycerol molecules are represented by their carbon atoms in the backbone (black spheres).The snapshots show (Figure 3a) groups of water molecules hydrogen bonded together, forming clusters in the solution. likewise, groups of glycerol molecules exist in glycerol-rich clusters. To quantitatively assess this nano-segregation, we completed a full cluster analysis for both glycerol and water across the concentration range, using the same method described previously [70]. Briefly, the cluster analysis is derived from the EPSR simulation of the scattering data (Figure 2) and provides structural insight into the connectivity of water molecules in the glycerol-water mixtures. A water cluster is defined by those water molecules that participate in a continuous hydrogen bonded network. To calculate the number of hydrogen bonded water molecules, we use local structure information from the RDF $g_{OW-OW}(r)$, which shows the probability of finding a water oxygen atom at a distance r from another water oxygen atom. Two water molecules are defined to be hydrogen bonded if the inter-oxygen contact distance if less than the radial distance of the first minimum of the RDF $g_{OW-OW}(r)$. The number of molecules in a water cluster is then counted for each of the snapshots in the EPSR simulation, generating a clusters size

distribution, which is the probability of finding a cluster of a particular size as a function of cluster size.
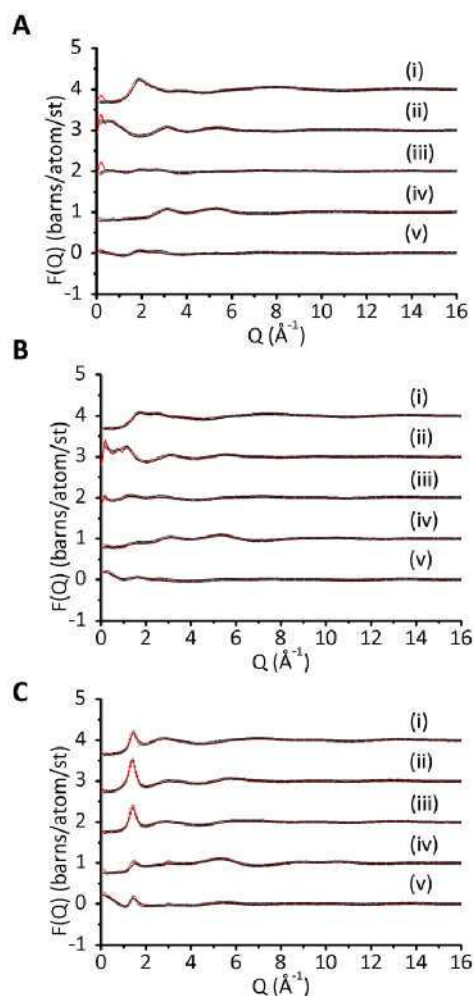
Figure 2: Experimental neutron diffraction structure factors F(Q) (black circles) and EPSR fitted structure factors (solid red lines) of glycerol–water solutions at concentration of mole fraction of glycerol (A) x_g = 0.10 at 262 K , (B) x_g = 0.25 at 238 K and (C) x_g = 0.80 at 285 K, for each of the isotopic substitutions (i) Glycerol-D8-D2O (ii) Glycerol-D5-H2O, (iii) Glycerol-D5HD3-HDO, (iv) Glycerol-H8-H2O and (v) Glycerol-HD8-HDO. The data shown here confirm that the EPSR model is in good agreement with the experimental data.
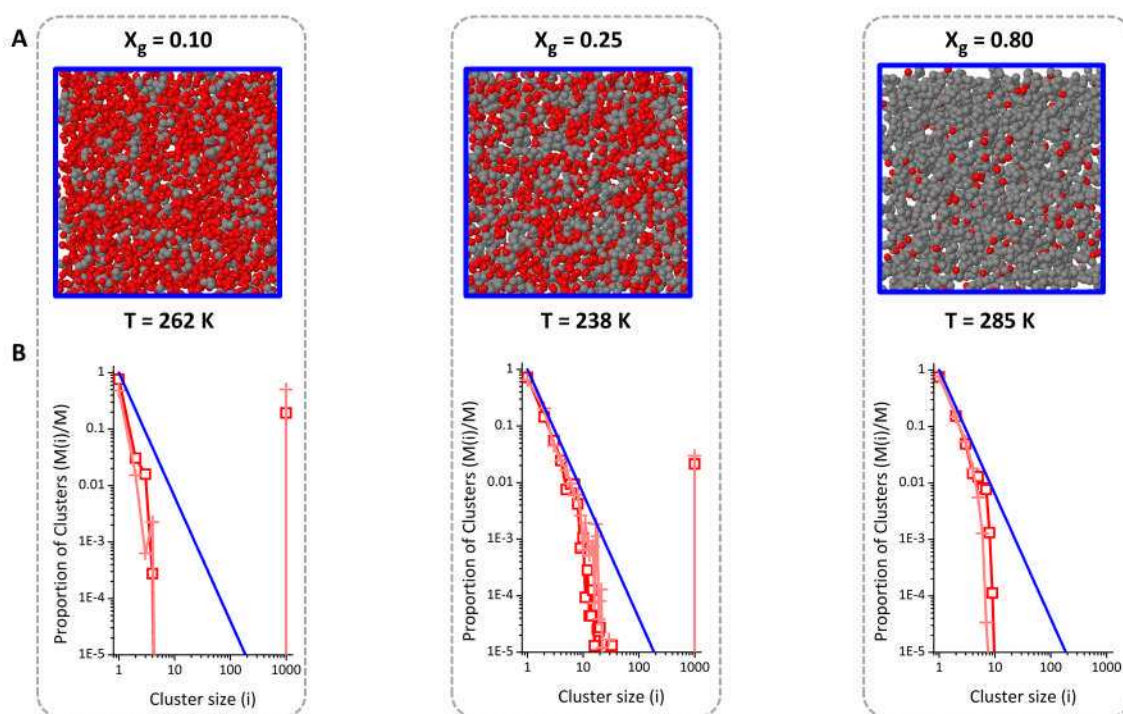
Figure 3: Structure of glycerol-water mixtures at low temperatures. Snapshots of the EPSR simulation box showing only glycerol-carbon (grey) and water-oxygen atoms (red) at each of the glycerol–water concentrations studied. From left to right, $x_g = 0.10$ at 262 K, $x_g = 0.25$ at 238 K and $x_g = 0.80$ at 285 K. The molecular scale segregation is shown by clusters of glycerol (grey) and water (red) molecules. (b) Cluster size distributions for water molecules at each of the glycerol–water concentrations studied at low temperatures (red squares and lines). Also shown for comparison are the cluster size distributions for water molecules at each of the glycerol–water concentrations studied at room temperatures (pink crosses and lines). The random 3-dimensional percolation threshold (blue line). These data show that water clusters are percolating (shown by red data points to the right of the blue line) at concentrations $x_g = 0.1$ and 0.25, but not at $x_g = 0.80$.

To quantitatively assess this nano-segregation, we completed a full cluster analysis for both glycerol and water across the concentration range, using the same method described previously.[70] Briefly, the cluster analysis is derived from the EPSR simulation of the scattering data (Figure 2) and provides structural insight into the connectivity of water molecules in the glycerol-water mixtures. A water cluster is defined by those water molecules that participate in a continuous hydrogen bonded network. To calculate the number of hydrogen bonded water molecules, we use local structure information from the RDF $g_{OW-OW}(r)$, which shows the probability of finding a water oxygen atom at a distance r from another water oxygen atom. Two water molecules are defined to be hydrogen bonded (and therefore in the same cluster) if the inter-oxygen contact distance if less than the radial distance of the first minimum of the RDF $g_{OW-OW}(r)$, 2.76 Å. The number of molecules in a water cluster is then counted for each of the snapshots in the EPSR simulation, generating a cluster size distribution, which is the probability of finding a cluster of a particular size as a function of cluster size.

Our previous studies on glycerol-water mixtures at room temperature showed that the molecules nano-segregate to form water-rich and glycerol-rich clusters. These regions exist as hydrogen bonded clusters which differ in size across the concentration range. Figure 3b shows the cluster distributions for the 3 glycerol-water systems studied here at low temperature; $x_g = 0.10$ at 262 K, $x_g = 0.25$ at 238 K

and $x_g = 0.80$ at 285 K (red squares and lines). For comparison, the data at room temperature for each concentration is also shown (Figure 3b, pink cross). Each plot shows the proportion of clusters containing i water molecules as a fraction of the total number of clusters, $M(i)/M$, (where $M = \Sigma_i M(i)$) against the water cluster size, I (see Supporting Info). Also shown on each plot is the random 3-dimensional percolation threshold (solid blue line), given by the power law $N = S^{-2.2}$, where N is the cluster proportion and S is the size of the cluster.[85] A water cluster is defined as percolating if it crosses the percolation threshold.

For the concentrated mixture, $x_g = 0.80$ at 285 K, water clusters range on size from 2 – 10 water molecules and do not cross the percolation threshold. This is similar to that which was found for $x_g = 0.80$ at room temperature.[70] As before, while glycerol molecules hydrogen bond to form a percolating network at this concentration, water molecules exist as small clusters. Further inspection of the water clusters reveals that while ~55 % of water exists as isolated water molecules, 45 % exist as part of hydrogen bonded water clusters. At the lower temperature of 262 K, the more dilute glycerol-water mixture $x_g = 0.10$ displays the opposite water clusters distribution. In this mixture, water molecules participate in a large, percolating cluster of size at least 999 molecules (Figure 3b, red square). This cluster spans the size of the system with ~99 % water molecules participating. This large, percolating water cluster was also observed in the room temperature experiments on this mixture (Figure 3b, pink cross).[70] At the lowest temperature studied here of 238 K, the

5

intermediate range glycerol-water mixture x_g = 0.25 displays a percolating water cluster (Figure 3b, red cross), again in agreement with room temperature experiments (Figure 3b, pink cross).[70] At this low temperature, ~3 % of water exists as isolated water molecules, ~3 % as part of small water clusters of size 2- 30, while the majority (94 %) exist as part of a large, percolating cluster. The cluster analysis confirms that for the 3 glycerol-water mixtures studied, x_g = 0.80 at 285 K, x_g = 0.10 at 262 K, and x_g = 0.25 at 238 K, water exists as part of a nano-segregated mixture. For x_g = 0.80 the water exists as isolated small clusters, while for the intermediate and dilute mixture x_g = 0.10 and x_g = 0.25 it exists as part of both small and large, percolating clusters. Given the presence of water within water clusters, we next examined the structure of water at low temperature.

Water structure at temperatures of 285 K, 262 K and 238 K

We determined the local water structure in glycerol-water mixtures at low temperature by examining the distribution for water oxygen-water oxygen pairs. From the EPSR molecular ensembles, we derived the site-site radial distribution functions (RDFs) $g_{O_wO_w}(r)$, which describes the relative density of water oxygen O_w, as a function of distance, r, from another water oxygen O_w (Figure 4a). Given that we will be examining the structure of water in detail, we also obtained the structure of pure water at room temperature and ambient pressure. Using previously completed neutron diffraction data on pure water[86] we completed EPSR simulations using the methods described to obtain an ensemble of three-dimensional molecular configurations with average structural correlations which are consistent with the diffraction data. The $g_{O_wO_w}(r)$ is shown in Figure 4b for pure water, x_g = 0.00 at 298 K, x_g = 0.80 at 285 K (solid line) and 298 K (dashed line), x_g = 0.10 at 262 K (solid line) and 298 K (dashed line) and x_g = 0.25 at 262 K (solid line) and 298 K (dashed line). The dashed lines in Figure 4b mark the positions of the 1st and 2nd coordination shall peak positions for pure water at 298 K, for comparison.
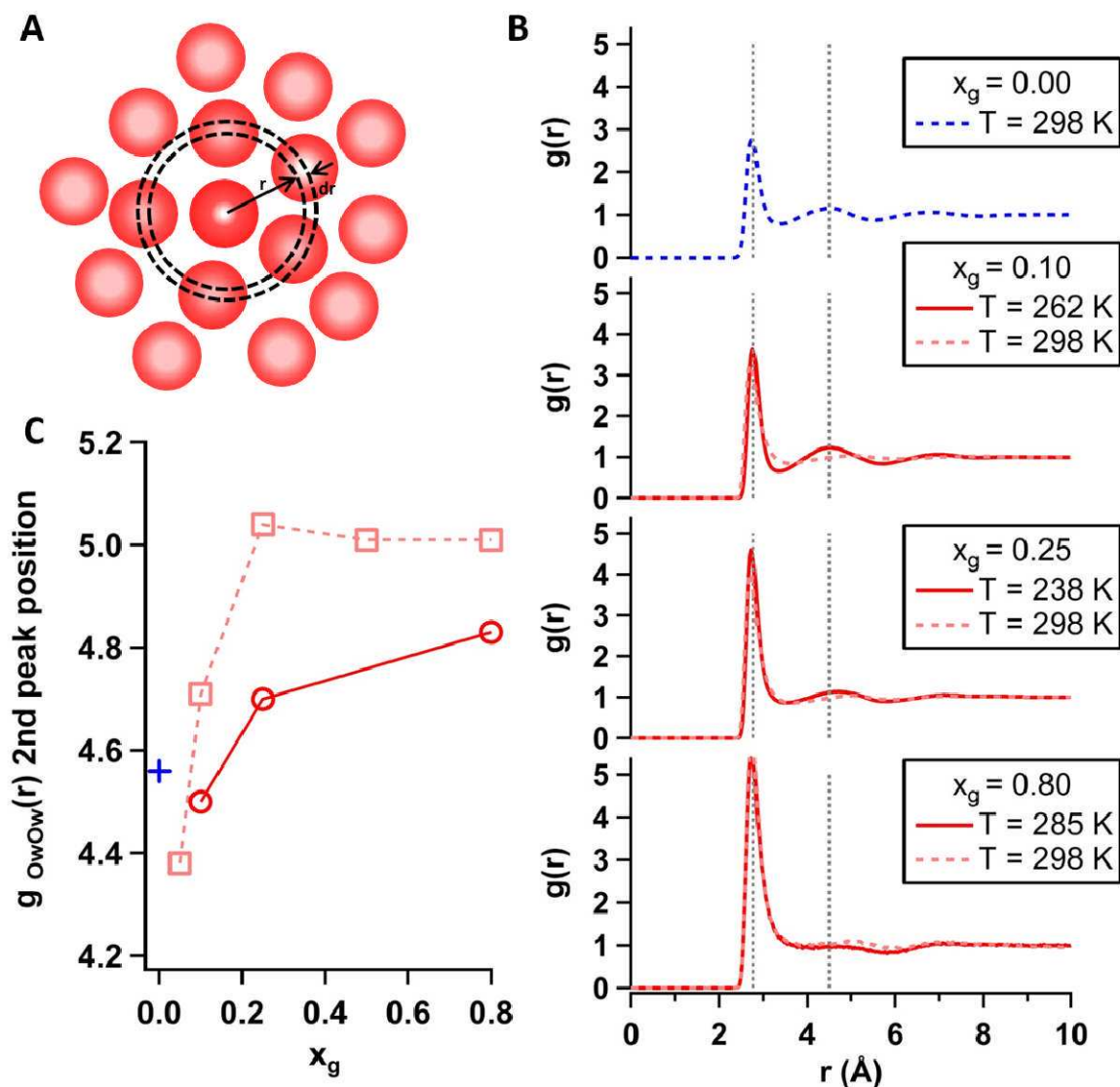

Figure 4: Water structure in glycerol-water mixtures at low temperature. (A) Schematic of the calculation involved for a site-site radial distribution functions (RDFs) $g_{\alpha\beta}(r)$, which describe the relative density of one type of atom, type, α, as a function

6

of distance, r, from another atom type, β. (B) RDFs for the water oxygen–water oxygen pairs $g_{OwOw}(r)$, that form hydrogen bonds in pure water at 298 K (upper) and in glycerol–water solutions; x_g = 0.10 at 262 K (solid line) and 298 K (dashed line), x_g = 0.25 at 262 K (solid line) and 298 K (dashed line) and x_g = 0.80 at 285 K (solid line) and 298 K (dashed line).. The RDFs are taken from the EPSR analysis of neutron diffraction data for each mixture. (C) The $g_{OwOw}(r)$ second coordination shell peak position is shown for glycerol-water mixtures at low temperature (red circles) and at room temperature (pink squares). The blue cross indicates the peak position found in pure water at 298 K.

As expected for pure water, the 1st and 2nd coordination peak positions are at 2.76 Å and 4.56 Å respectively. For each of the 3 low temperature glycerol-water mixtures (solid line in Figure 3b) the first peak position remains relatively unchanged, as observed previously for glycerol-water at 298 K. The position of the second peak in $g_{OwOw}(r)$ in the glycerol–water solutions shows, however, much larger deviations when compared with that of pure water. First, we present the previously studied room temperature distributions.[70-71] At the dilute concentration of x_g = 0.10 at room temperature the second peak position shifts outwards from 4.56 Å in pure water to 4.71 Å. This increases to 5.04 Å at the intermediate concentration of x_g = 0.25 at room temperature, while at x_g = 0.80 at room temperature the second coordination shell becomes much broader with a peak at ~ 5.5 Å. Upon lowering of the temperature all 3 RDFs $g_{OwOw}(r)$ become sharper and more well defined (Figure 4b, solid lines). The second peak position appears to shift inwards slightly, relative to the room temperature mixture. This inward shift in the second peak position of $g_{OwOw}(r)$ returns the water structure to a more similar position to that measured for pure water at 298 K, particularly for x_g = 0.10 at 262 K.

To examine this in more detail, we compare the $g_{OwOw}(r)$ second peak position for all previously studied glycerol-water mixtures at room temperature,[70-71] as well as for the 3 low temperature mixtures studied here. Figure 4c shows the $g_{OwOw}(r)$ second peak position for room temperature glycerol-water (red squares) and low temperature glycerol-water (red circles). For reference, the $g_{OwOw}(r)$ second peak position for pure water at 298 K is shown as a blue cross. It can be seen from Figure 4c that an increasing quantity of glycerol at room temperature results in an increasing $g_{OwOw}(r)$ second peak position, while a reduction in the temperature reduces this impact. Interestingly, the glycerol water mixture which is most similar to that of pure water at 298 K is x_g = 0.10 at 262 K. The position of the second peak position in the water $g_{OwOw}(r)$ is often suggested as an indicator of the tetrahedrality (or lack thereof) within a system. In this next section we measure the tetrahedrality in the glycerol-water system.

Local tetrahedral ordering of water at low temperature
We further examined the water structure in the glycerol-water mixtures at low temperature by measuring the triplet bond angle distribution of water oxygen atoms. This method measures the angular distribution of water oxygen atoms in the mixture. The tetrahedrality of the water network can be quantified by measuring the included angle formed by three water oxygen atoms (Figure 5a). Here, the included angle is measured for all triplets of atoms, which conform to specific distance criteria. The separation cut-off is set as the radial distance of the first minimum in the relevant water oxygen RDF $g_{OwOw}(r)$ (Figure 4b). This distribution, N N(θ) is then divided by sin (θ) to produce the density of triplet angles P(θ). In Figure 5b the proportion of included angles formed by water oxygen triplets (Ow-Ow-Ow) as a function of angle θ is shown for pure water x_g = 0.0 at 298 K (blue solid line) and 280K

(blue dashed line). The triplet bond angle distribution is also shown for each of the 3 glycerol-water mixtures; x_g = 0.80 at 285 K (red solid line) and 298 K (red dashed line), x_g = 0.10 at 262 K (red solid line) and 298 K (red dashed line) and x_g = 0.25 at 262 K (red solid line) and 298 K (red dashed line). The black dashed line in Figure 5B indicates the position of perfect tetrahedrality (θ = 109.5°).

Considering the pure water distribution at 298 K (blue solid line in Figure 5b), a small peak is observed at ~ 50° and at larger angles a broader distribution is found with a peak at 104°. The small peak is attributed to oxygen atoms that are within the first coordination shell of another oxygen atom, but do not form hydrogen bonds. These oxygen atoms are known as interstitial atoms as they occupying space within the first coordination shall but are not forming hydrogen bonds to the central oxygen atoms. The second peak indicates hydrogen bonded oxygen triplets, as depicted in Figure 5a. Upon cooling pure water to 280 K, the proportion of interstitial oxygen atoms decreases, while the proportion of hydrogen bonded waters increases slightly (Figure 5b, blue dashed line). Next we consider the triplet bond angle distributions in glycerol-water mixtures.

Examination of the triplet bond angle distribution for x_g = 0.80 at 285 K shows that the hydrogen bonded network is broken at high glycerol concentrations (Figure 5b, red solid line) marked by an absence in a prominent peak around 104°. This absence was also observed at 298 K (Figure 5B red dashed line). There is also an increase in the peak at 50° at both 285 K and 298 K. The increased presence of interstitial oxygen atoms suggests that the connectivity of the water network is diminished at this concentration. For x_g = 0.10 at 262 K the triplet bond angle distribution displays a well-defined peak at large values of θ, indicating the presence of a prominent hydrogen bonded network. Comparison of the low temperature data to that at room temperature shows that at the dilute concentration of x_g = 0.10 there is an increase in the proportion of water oxygen triplets that have an angle around that of a perfect tetrahedral angle (Figure 5b, black dashed line), at the expense of interstitial water atoms. For x_g = 0.25 at 238 K the triplet bond angle distribution again displays a well-defined peak at large angles. Interestingly, the peak position of water oxygen triplet in x_g = 0.25 at the low temperature of 238 K is much closer to that of a perfect tetrahedrality (θ = 109.5°), than that of pure water at 298 K (Figure 5b, blue solid line)

To quantify the degree of tetrahedrality in the glycerol-water mixtures we used a method described previously.[87] Briefly, the tetrahedral nature of a system can be quantified using tetrahedral order parameters. One such order parameter is the q-factor, proposed by Errington and Debenedetti,[87] where the q-factor is defined as;

7

$$q = 1 - \frac{9}{4} \frac{\int_0^\pi P(\theta)(\cos\theta + \frac{1}{2})^2 \sin\theta d\theta}{\int_0^\pi P(\theta)\sin\theta d\theta}$$

Where the q-factor has been rescaled such that q = 1 for a perfect tetrahedral system and q = 0 for an ideal gas distribution. The values of the q-factors have been calculated for each of the water oxygen triplets shown in Figure 5b for the glycerol-water mixtures at low temperature and at 298 K, as well as for pure water at a range of different temperatures. Figure 5c shows the calculated q-factors for $x_g = 0.80$ at 285 K (red bar) and 298 K (pink bar), $x_g = 0.10$ at 262 K (red bar) and 298 K (pink bar) and $x_g = 0.25$ at 262 K (red bar) and 298 K (pink bar). The calculated q-factors for water are also shown for temperatures ranging from 280 K to 365 K (blue bars). From Figure 5c (upper) it can be seen that the q-factor increases at low temperature for each of the 3 glycerol-water mixtures, relative to their room temperature equivalent. This increase in the q-factor is more dramatic than that observed for pure water, as the temperature is decreased (Figure 5c, lower). From this data it can be concluded that the water network in both $x_g = 0.10$ at 262 K and $x_g = 0.25$ at 262 K is closer to being tetrahedral than the mixture at room temperature. In the case of $x_g = 0.10$ at 262 K, the tetrahedrality is greater than that of liquid water at 280 K. To calculate the average local density around any given water molecule we have employed a method described previously.[24] The data show that the local density of water oxygen atoms is ~0.0146 molecules/Å^3, which is significantly lower than the bulk value of ~0.0334 molecules/ Å^3 (Figure S1).
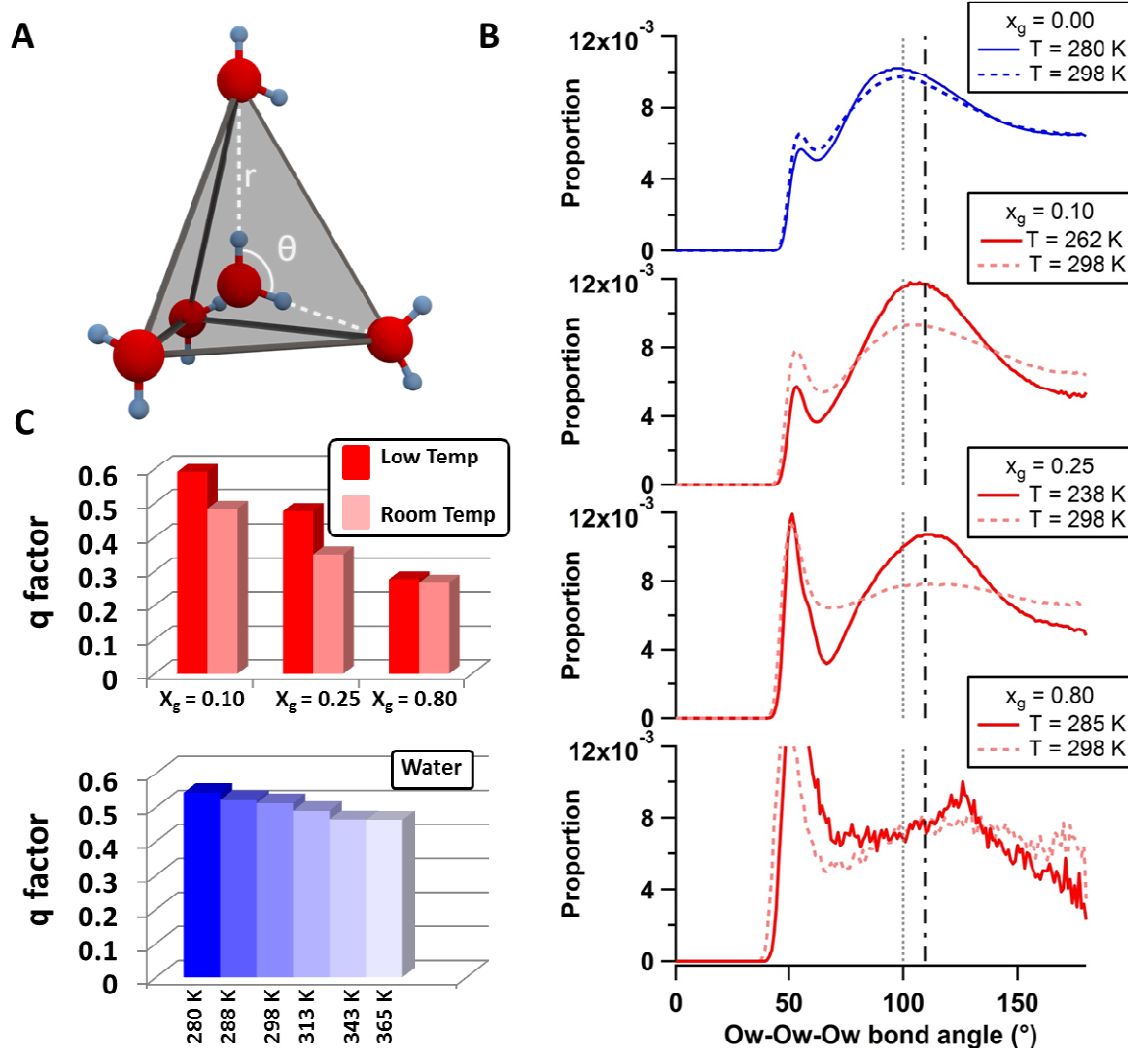
Figure 5 Tetrahedrality in water structure. (A) (B) The proportion of water oxygen triplets that form an included angle, as a function of bond angle θ. Data are shown for pure water $x_g = 0.0$ at 298 K (blue solid line) and 280K (blue dashed line), and for each of the 3 glycerol-water mixtures; $x_g = 0.10$ at 262 K (solid line) and 298 K (dashed line), $x_g = 0.25$ at 262 K (solid line) and 298 K (dashed line) and $x_g = 0.80$ at 285 K (solid line) and 298 K (dashed line). The grey dotted line denotes the location of the peak position in pure water at 298 K, while the black dashed line indicates the perfect tetrahedral angle of 109.5°. (C) The calculated Q-factor for each of the glycerol-water mixtures at room temperature and low temperature

CONCLUSIONS

Our neutron diffraction experiments and EPSR simulation results confirm that glycerol-water mixtures nano-segregate into regions of glycerol-rich and water-rich clusters in the stable liquid region at low temperatures. At the low glycerol concentrations of $x_g = 0.10$ and 0.25 an extended, hydrogen bonded network exists which spans the simulation box (Figure 2b). We find that the degree of clustering at the low temperatures studied here is relatively unchanged compared with that previously measured at room temperature (Figure 3b). Thus, nano-segregation in a glycerol-water solution is prevalent at both ambient and low temperatures. Nano-segregation in binary liquids is not unique to glycerol-water mixtures and has previously been observed in other systems using neutron diffraction; including methanol-water,[72] tertiary butanol-water[88] and sorbitol-water.[89] In the case of methanol- and tertiary butanol-water mixtures an enhancement in nano-segregation was observed upon cooling.[90-91] In the present study we find that glycerol and water form hydrogen-bonded, glycerol-rich and water-rich clusters that are unchanged upon cooling.

While the degree of water clustering (Figure 3b) was not enhanced or depleted upon cooling, the local water structure was markedly affected (Figure 4). The second coordination shell peak was measured to sharpen (Figure 4B) and shift inwards upon cooling (Figure 4c) relative to the room temperature measurements, for all three glycerol-water mixtures studied. This inward shift of the second peak position was largest at $x_g = 0.25$, which is close to the concentration at which the glycerol-water mixture exhibits a minimum in the freezing point depression ($x_g = 0.28$, T 226.65 K).

Upon cooling, water becomes notably more tetrahedral in all three of the glycerol-water mixtures studied (Figure 5b). Examination of the liquid water structure in the nano-segregated system at $x_g = 0.25$ reveals that at the temperature studied (238 K) water forms a structure which is more tetrahedral that at room temperature. Thus, in a nano-segregated glycerol-water solution at low temperatures down to 238 K we measure a low density-like water structure, which exists as a more open, hydrogen-bonded tetrahedral structure, than the liquid under the same conditions at ambient temperature. We quantify the degree of tetrahedrality in the glycerol-water mixtures and measure an increase in the q-factor upon cooling for all three glycerol-water mixtures. The largest increase is seen for the $x_g = 0.25$ mixture, which is closest to the eutectic point, which shows an increase of 36 % in the q-factor for water, upon cooling from 298 K to 238 K. We hypothesis that at this concentration ($x_g = 0.25$) ice formation is prevented due to the water segregation (Figure 3a), where hydrogen-bonded water molecules are unable to form an extended water network. Water is then able to form an enhanced tetrahedral network which is 'protected' by an extensive and encapsulating glycerol interface (Figure S2).

This water structure is reminiscent of the structure of low density pure water, which has previously been observed experimentally and computationally. However, these studies explore low density water in either the *confined* or *metastable* states. In the present study we have access to low density water down to 238 K at *equilibrium*. The nano-segregated glycerol-water mixture therefore provides an attractive platform with which to further probe the structural properties of water at low temperatures. This includes the potential to look for liquid water polymorphism, which has received considerable attention due its importance in the LLCP scenario, in a thermodynamically stable phase.

AUTHOR INFORMATION
Corresponding Author
L.Dougan@leeds.ac.uk

REFERENCES

1.   Ball, P. *Life's Matrix: A Biography of Water.* University of California Press: 1999.
2.   Ball, P. Water as an Active Constituent in Cell Biology. *Chem Rev* **2008,** *108*, 74-108.
3.   Mojzsis, S. J.; Harrison, T. M.; Pidgeon, R. T. Oxygen-Isotope Evidence from Ancient Zircons for Liquid Water at the Earth's Surface 4,300 Myr Ago. *Nature* **2001,** *409*, 178-181.
4.   Dudgeon, D., et al. Freshwater Biodiversity: Importance, Threats, Status and Conservation Challenges. *Biol Rev* **2006,** *81*, 163-182.
5.   Angell, C. A. *Water: A Comprehensive Treatise.* Plenum: New York, 1982; Vol. 7.
6.   Debenedetti, P. G. Metastable Liquids. Princeton University Press: 1996.
7.   Debenedetti, P. G. Supercooled and Glassy Water. *J Phys-Condens Mat* **2003,** *15*, R1669-R1726.

8.   Mishima, O.; Stanley, H. E. The Relationship between Liquid, Supercooled and Glassy Water. *Nature* **1998,** *396*, 329-335.
9.   Poole, P. H.; Sciortino, F.; Essmann, U.; Stanley, H. E. Phase-Behavior of Metastable Water. *Nature* **1992,** *360*, 324-328.
10.   Chen, S. H.; Mallamace, F.; Mou, C. Y.; Broccio, M.; Corsaro, C.; Faraone, A.; Liu, L. The Violation of the Stokes-Einstein Relation in Supercooled Water. *P Natl Acad Sci USA* **2006,** *103*, 12974-12978.
11.   Fanetti, S.; Lapini, A.; Pagliai, M.; Citroni, M.; Di Donato, M.; Scandolo, S.; Righini, R.; Bini, R. Structure and Dynamics of Low-Density and High-Density Liquid Water at High Pressure. *J Phys Chem Lett* **2014,** *5*, 235-240.
12.   Huang, C., et al. The Inhomogeneous Structure of Water at Ambient Conditions. *P Natl Acad Sci USA* **2009,** *106*, 15214-15218.
13.   Liu, L.; Chen, S. H.; Faraone, A.; Yen, C. W.; Mou, C. Y. Pressure Dependence of Fragile-to-Strong Transition and a Possible Second Critical Point in Supercooled Confined Water. *Phys Rev Lett* **2005,** *95*, 117802-117804.

14. Mallamace, F.; Branca, C.; Broccio, M.; Corsaro, C.; Mou, C. Y.; Chen, S. H. The Anomalous Behavior of the Density of Water in the Range 30k < T < 373k. *P Natl Acad Sci USA* **2007,** *104,* 18387-18391.

15. Mallamace, F.; Broccio, M.; Corsaro, C.; Faraone, A.; Liu, L.; Mou, C. Y.; Chen, S. H. Dynamical Properties of Confined Supercooled Water: An Nmr Study. *J Phys-Condens Mat* **2006,** *18,* S2285-S2297.

16. Mallamace, F.; Broccio, M.; Corsaro, C.; Faraone, A.; Majolino, D.; Venuti, V.; Liu, L.; Mou, C. Y.; Chen, S. H. Evidence of the Existence of the Low-Density Liquid Phase in Supercooled, Confined Water. *P Natl Acad Sci USA* **2007,** *104,* 424-428.

17. Mallamace, F.; Broccio, M.; Corsaro, C.; Faraone, A.; Wanderlingh, U.; Liu, L.; Mou, C. Y.; Chen, S. H. The Fragile-to-Strong Dynamic Crossover Transition in Confined Water: Nuclear Magnetic Resonance Results. *J Chem Phys* **2006,** *124,* 161102-161107.

18. Soper, A. K.; Ricci, M. A. Structures of High-Density and Low-Density Water. *Phys Rev Lett* **2000,** *84,* 2881-2884.

19. Borick, S. S.; Debenedetti, P. G.; Sastry, S. A Lattice Model of Network-Forming Fluids with Orientation-Dependent Bonding - Equilibrium, Stability, and Implications for the Phase-Behavior of Supercooled Water. *J Phys Chem-Us* **1995,** *99,* 3781-3792.

20. Poole, P. H.; Sciortino, F.; Grande, T.; Stanley, H. E.; Angell, C. A. Effect of Hydrogen-Bonds on the Thermodynamic Behavior of Liquid Water. *Phys Rev Lett* **1994,** *73,* 1632-1635.

21. Limmer, D. T.; Chandler, D. The Putative Liquid-Liquid Transition Is a Liquid-Solid Transition in Atomistic Models of Water. *J Chem Phys* **2011,** *135,* 134503-134510.

22. Mallamace, F. The Liquid Water Polymorphism. *P Natl Acad Sci USA* **2009,** *106,* 15097-15098.

23. Mishima, O.; Calvert, L. D.; Whalley, E. An Apparently 1st-Order Transition between 2 Amorphous Phases of Ice Induced by Pressure. *Nature* **1985,** *314,* 76-78.

24. Soper, A. K. Radical Re-Appraisal of Water Structure in Hydrophilic Confinement. *Chemical Physics Letters* **2013,** *590,* 1-15.

25. Leng, Y. S.; Cummings, P. T. Hydration Structure and Shear Viscosity of Water Nanoconfined between Mica Surfaces. *Proceedings of the Asme Fluids Engineering Division Summer Conference, Vol 2* **2006,** 505-510.

26. Gordillo, M. C.; Nagy, G.; Marti, J. Structure of Water Nanoconfined between Hydrophobic Surfaces. *J Chem Phys* **2005,** *123,* 54707-54709.

27. Soper, A. K. Density Minimum in Supercooled Confined Water. *P Natl Acad Sci USA* **2011,** *108,* E1192-E1192.

28. Zhang, Y.; Faraone, A.; Kamitakahara, W. A.; Liu, K. H.; Mou, C. Y.; Leao, J. B.; Chang, S.; Chen, S. H. Density Hysteresis of Heavy Water Confined in a Nanoporous Silica Matrix. *P Natl Acad Sci USA* **2011,** *108,* 12206-12211.

29. Clark, G. N. I.; Hura, G. L.; Teixeira, J.; Soper, A. K.; Head-Gordon, T. Small-Angle Scattering and the Structure of Ambient Liquid Water. *P Natl Acad Sci USA* **2010,** *107,* 14003-14007.

30. Sellberg, J. A., et al. Ultrafast X-Ray Probing of Water Structure Below the Homogeneous Ice Nucleation Temperature. *Nature* **2014,** *510,* 381-384.

31. Soper, A. K. Supercooled Water Continuous Trends. *Nat Mater* **2014,** *13,* 671-673.

32. Fanetti, S.; Pagliai, M.; Citroni, M.; Lapini, A.; Scandolo, S.; Righini, R.; Bini, R. Connecting the Water Phase Diagram to the Metastable Domain: High-Pressure Studies in the Supercooled Regime. *J Phys Chem Lett* **2014,** *5,* 3804-3809.

33. Suzuki, Y.; Mishima, O. Experimentally Proven Liquid-Liquid Critical Point of Dilute Glycerol-Water Solution at 150 K. *J Chem Phys* **2014,** *141,* 94505-94509.

34. Bellissentfunel, M. C.; Bosio, L. A Neutron-Scattering Study of Liquid D2o under Pressure and at Various Temperature. *J Chem Phys* **1995,** *102,* 3727-3735.

35. Fuller, B. J. Cryoprotectants: The Essential Antifreezes to Protect Life in the Frozen State. *Cryoletters* **2004,** *25,* 375-388.

36. Chelli, R.; Procacci, P.; Cardini, G.; Califano, S. Glycerol Condensed Phases Part Ii. A Molecular Dynamics Study of the Conformational Structure and Hydrogen Bonding. *Phys Chem Chem Phys* **1999,** *1,* 879-885.

37. Lane, L. B. Freezing Points of Glycerol and Its Aqueous Solutions. *Ind Eng Chem* **1925,** *17,* 924-924.

38. Lovelock, J. E. The Mechanism of the Protective Action of Glycerol against Haemolysis by Freezing and Thawing. *Biochimica Et Biophysica Acta* **1953,** *11,* 28-36.

39. Okazaki, T.; Abe, S.; Shimada, M. Improved Conception Rates in Sows Inseminated with Cryopreserved Boar Spermatozoa Prepared with a More Optimal Combination of Osmolality and Glycerol in the Freezing Extender. *Animal Science Journal* **2009,** *80,* 121-129.

40. Zachariassen, K. E.; Kristiansen, E. Ice Nucleation and Antinucleation in Nature. *Cryobiology* **2000,** *41,* 257-279.

41. Zhang, H.; Grinstaff, M. W. Recent Advances in Glycerol Polymers: Chemistry and Biomedical Applications. *Macromol Rapid Comm* **2014,** *35,* 1906-1924.

42. Sonnati, M. O.; Amigoni, S.; de Givenchy, E. P. T.; Darmanin, T.; Choulet, O.; Guittard, F. Glycerol Carbonate as a Versatile Building Block for Tomorrow: Synthesis, Reactivity, Properties and Applications. *Green Chem* **2013,** *15,* 283-306.

43. Rywinska, A.; Juszczyk, P.; Wojtatowicz, M.; Robak, M.; Lazar, Z.; Tomaszewska, L.; Rymowicz, W. Glycerol as a Promising Substrate for Yarrowia Lipolytica Biotechnological Applications. *Biomass Bioenerg* **2013,** *48,* 148-166.

44. Gu, Y. L.; Jerome, F. Glycerol as a Sustainable Solvent for Green Chemistry. *Green Chem* **2010,** *12,* 1127-1138.

45. Polge, C.; Smith, A. U.; Parkes, A. S. Revival of Spermatozoa after Vitrification and Dehydration at Low Temperatures. *Nature* **1949,** *164,* 666-666.

46. Chelli, R.; Gervasio, F. L.; Gellini, C.; Procacci, P.; Cardini, G.; Schettino, V. Density Functional Calculation of Structural and Vibrational Properties of Glycerol. *J Phys Chem A* **2000,** *104,* 5351-5357.

47. Chelli, R.; Procacci, P.; Cardini, G.; Della Valle, R. G.; Califano, S. Glycerol Condensed Phases Part I. A Molecular Dynamics Study. *Phys Chem Chem Phys* **1999,** *1,* 871-877.

48. Chen, C.; Li, W. Z.; Song, Y. C.; Yang, J. Hydrogen Bonding Analysis of Glycerol Aqueous Solutions: A Molecular Dynamics Simulation Study. *J Mol Liq* **2009,** *146,* 23-28.

49. Kyrychenko, A.; Dyubko, T. S. Molecular Dynamics Simulations of Microstructure and Mixing Dynamics of Cryoprotective Solvents in Water and in the Presence of a Lipid Membrane. *Biophysical Chemistry* **2008,** *136,* 23-31.

50. MacKerell, A. D., et al. All-Atom Empirical Potential for Molecular Modeling and Dynamics Studies of Proteins. *Journal of Physical Chemistry B* **1998,** *102,* 3586-3616.

51. Blieck, J.; Affouard, F.; Bordat, P.; Lerbret, A.; Descamps, M. Molecular Dynamics Simulations of Glycerol Glass-Forming Liquid. *Chem Phys* **2005,** *317,* 253-257.

52. Busselez, R.; Lefort, R.; Ji, Q.; Affouard, F.; Morineau, D. Molecular Dynamics Simulation of Nanoconfined Glycerol. *Phys Chem Chem Phys* **2009,** *11,* 11127-11133.

53. Chen, C.; Li, W. Z. Molecular Dynamics Simulation of Hydrogen Bonding Characteristics in Aqueous Glycerol Solutions. *Acta Phys-Chim Sin* **2009,** *25,* 507-512.

54. Dirama, T. E.; Carri, G. A.; Sokolov, A. P. Role of Hydrogen Bonds in the Fast Dynamics of Binary Glasses of Trehalose and Glycerol: A Molecular Dynamics Simulation Study. *J Chem Phys* **2005,** *122,* 114505-114508.

55. Egorov, A. V.; Lyubartsev, A. P.; Laaksonen, A. Molecular Dynamics Simulation Study of Glycerol-Water Liquid Mixtures. *Journal of Physical Chemistry B* **2011,** *115,* 14572-14581.

56. Perova, T. S.; Rasmussen, U.; Nielsen, O. F.; Kirillov, S. A.; Christensen, D. H.; Vij, J. K. Low-Frequency Studies and Molecular Dynamics of Water/Glycerol Mixtures. *Spectroscopy of Biological Molecules: New Directions* **1999,** 685-686.

57. Root, L. J.; Berne, B. J. Effect of Pressure on Hydrogen Bonding in Glycerol: A Molecular Dynamics Investigation. *J Chem Phys* **1997,** *107,* 4350-4357.

58. Root, L. J.; Stillinger, F. H. Short-Range Order in Glycerol - a Molecular-Dynamics Study. *J Chem Phys* **1989,** *90,* 1200-1208.

59. Weng, L. D.; Chen, C.; Zuo, J. G.; Li, W. Z. Molecular Dynamics Study of Effects of Temperature and Concentration on Hydrogen-Bond Abilities of Ethylene Glycol and Glycerol: Implications for Cryopreservation. *J Phys Chem A* **2011,** *115,* 4729-4737.

60. Yongye, A. B.; Foley, B. L.; Woods, R. J. On Achieving Experimental Accuracy from Molecular Dynamics Simulations of Flexible Molecules: Aqueous Glycerol. *J Phys Chem A* **2008,** *112,* 2634-2639.

61. Zhang, N.; Li, W. Z.; Chen, C.; Zuo, J. G.; Weng, L. D. Molecular Dynamics Investigation of the Effects of Concentration on Hydrogen Bonding in Aqueous Solutions of Methanol, Ethylene Glycol and Glycerol. *B Korean Chem Soc* **2013,** *34,* 2711-2719.

62. Zhang, N.; Li, W. Z.; Chen, C.; Zuo, J. G.; Weng, L. D. Molecular Dynamics Study on Water Self-Diffusion in Aqueous Mixtures of Methanol, Ethylene Glycol and Glycerol: Investigations from the Point of View of Hydrogen Bonding. *Mol Phys* **2013,** *111,* 939-949.

63. Akinkunmi, F. O.; Jahn, D. A.; Giovambattista, N. Effects of Temperature on the Thermodynamic and Dynamical Properties of Glycerol-Water Mixtures: A Computer Simulation Study of Three Different Force Fields. *Journal of Physical Chemistry B* **2015,** *119,* 6250-6261.

64. Jahn, D. A.; Akinkunmi, F. O.; Giovambattista, N. Effects of Temperature on the Properties of Glycerol: A Computer Simulation Study of Five Different Force Fields. *Journal of Physical Chemistry B* **2014,** *118,* 11284-11294.

65. Dashnau, J. L.; Nucci, N. V.; Sharp, K. A.; Vanderkooi, J. M. Hydrogen Bonding and the Cryoprotective Properties of Glycerol/Water Mixtures. *Journal of Physical Chemistry B* **2006,** *110,* 13670-13677.

10

66.   Kataoka, Y.; Kitadai, N.; Hisatomi, O.; Nakashima, S. Nature of Hydrogen Bonding of Water Molecules in Aqueous Solutions of Glycerol by Attenuated Total Reflection (Atr) Infrared Spectroscopy. *Appl Spectrosc* **2011**, *65*, 436-441.

67.   Towey, J. J.; Dougan, L. Structural Examination of the Impact of Glycerol on Water Structure. *Journal of Physical Chemistry B* **2012**, *116*, 1633-1641.

68.   Towey, J. J.; Soper, A. K.; Dougan, L. The Structure of Glycerol in the Liquid State: A Neutron Diffraction Study. *Phys Chem Chem Phys* **2011**, 9397-9406.

69.   Towey, J. J.; Soper, A. K.; Dougan, L. Preference for Isolated Water Molecules in a Concentrated Glycerol-Water Mixture. *Journal of Physical Chemistry B* **2011**, *115*, 7799-7807.

70.   Towey, J. J.; Soper, A. K.; Dougan, L. Molecular Insight into the Hydrogen Bonding and Micro-Segregation of a Cryoprotectant Molecule. *Journal of Physical Chemistry B* **2012**, *116*, 13898-13904.

71.   Towey, J. J.; Soper, A. K.; Dougan, L. What Happens to the Structure of Water in Cryoprotectant Solutions? *Faraday Discuss* **2013**, *167*, 159-176.

72.   Dougan, L.; Bates, S. P.; Hargreaves, R.; Fox, J. P.; Crain, J.; Finney, J. L.; Reat, V.; Soper, A. K. Methanol-Water Solutions: A Bi-Percolating Liquid Mixture. *J Chem Phys* **2004**, *121*, 6456-6462.

73.   Dougan, L.; Crain, J.; Finney, J. L.; Soper, A. K. Molecular Self-Assembly in a Model Amphiphile System. *Phys Chem Chem Phys* **2010**, *12*, 10221-10229.

74.   Rhys, N. H.; Dougan, L. The Emerging Role of Hydrogen Bond Interactions in Polyglutamine Structure, Stability and Association. *Soft Matter* **2013**, *9*, 2359-2364.

75.   Rhys, N. H.; Soper, A. K.; Dougan, L. The Hydrogen-Bonding Ability of the Amino Acid Glutamine Revealed by Neutron Diffraction Experiments. *Journal of Physical Chemistry B* **2012**, *116*, 13308-13319.

76.   McCune, J. A.; Turner, A. H.; Coleman, F.; White, C. M.; Callear, S. K.; Youngs, T. G. A.; Swadzba-Kwasny, M.; Holbrey, J. D. Association and Liquid Structure of Pyridine-Acetic Acid Mixtures Determined from Neutron Scattering Using a 'Free Proton' Epsr Simulation Model. *Phys Chem Chem Phys* **2015**, *17*, 6767-6777.

77.   Murphy, T.; Hayes, R.; Imberti, S.; Warr, G. G.; Atkin, R. Nanostructure of an Ionic Liquid-Glycerol Mixture. *Phys Chem Chem Phys* **2014**, *16*, 13182-13190.

78.   Sillren, P.; Swenson, J.; Mattsson, J.; Bowron, D.; Matic, A. The Temperature Dependent Structure of Liquid 1-Propanol as Studied by Neutron Diffraction and Epsr Simulations. *J Chem Phys* **2013**, *138*, 214501-214509.

79.   Busch, S.; Pardo, L. C.; O'Dell, W. B.; Bruce, C. D.; Lorenz, C. D.; McLain, S. E. On the Structure of Water and Chloride Ion Interactions with a Peptide Backbone in Solution. *Phys Chem Chem Phys* **2013**, *15*, 21023-21033.

80.   Bowron, D. T.; Beret, E. C.; Martin-Zamora, E.; Soper, A. K.; Marcos, E. S. Axial Structure of the Pd(Ii) Aqua Ion in Solution. *J Am Chem Soc* **2012**, *134*, 962-967.

81.   Pagnotta, S. E.; McLain, S. E.; Soper, A. K.; Bruni, F.; Ricci, M. A. Water and Trehalose: Flow Much Do They Interact with Each Other? *Journal of Physical Chemistry B* **2010**, *114*, 4904-4908.

82.   Soper, A. K.; Howells, S.; Hannon, A. C. *Atlas - Analysis of Time-of-Flight Diffraction Data from Liquid and Amorphous Samples*; 1999.

83.   Soper, A. K. Partial Structure Factors from Disordered Materials Diffraction Data: An Approach Using Empirical Potential Structure Refinement. *Physical Review B* **2005**, *72*, 104204-104211.

84.   Robinson, G. W.; Zhu, S. B.; Singh, S.; Evans, M. W. *Water in Biology, Chemistry and Physics : Experimental Overviews and Computational Methodologies*. World Scientific: Singaore, 1996.

85.   Jan, N. Large Lattice Random Site Percolation. *Physica A* **1999**, *266*, 72-75.

86.   Soper, A. K. The Radial Distribution Functions of Water and Ice from 220 to 673 K and at Pressures up to 400 Mpa. *Chem Phys* **2000**, *258*, 121-137.

87.   Errington, J. R.; Debenedetti, P. G. Relationship between Structural Order and the Anomalies of Liquid Water. *Nature* **2001**, *409*, 318-321.

88.   Bowron, D. T.; Moreno, S. D. The Structure of a Concentrated Aqueous Solution of Tertiary Butanol: Water Pockets and Resulting Perturbations. *J Chem Phys* **2002**, *117*, 3753-3762.

89.   Chou, S. G.; Soper, A. K.; Khodadadi, S.; Curtis, J. E.; Krueger, S.; Cicerone, M. T.; Fitch, A. N.; Shalaev, E. Y. Pronounced Microheterogeneity in a Sorbitol-Water Mixture Observed through Variable Temperature Neutron Scattering. *Journal of Physical Chemistry B* **2012**, *116*, 4439-4447.

90.   Bowron, D. T.; Finney, J. L.; Soper, A. K. Structural Investigation of Solute-Solute Interactions in Aqueous Solutions of Tertiary Butanol. *Journal of Physical Chemistry B* **1998**, *102*, 3551-3563.

91.   Dougan, L.; Hargreaves, R.; Bates, S. P.; Finney, J. L.; Reat, V.; Soper, A. K.; Crain, J. Segregation in Aqueous Methanol Enhanced by Cooling and Compression. *J Chem Phys* **2005**, *122*, 174514-174517.

11